



Global Snow Monitoring for Climate Research

Algorithm Theoretical Basis Document – SWE-algorithm

EUROPEAN SPACE AGENCY STUDY CONTRACT REPORT
ESRIN Contract 21703/08/I-EC

DELIVERABLE 06

PREPARED BY

KARI LUOJUS, JOUNI PULLIAINEN, MATIAS TAKALA, JUHA LEMMETYINEN, MWABA KANGWA, TUOMO SMOLANDER (FMI); CHRIS DERKSEN (ENVIRONMENT CANADA)

GLOBSNOW CONSORTIUM

FINNISH METEOROLOGICAL INSTITUTE (FMI) - PRIME CONTRACTOR

ENVEO IT GMBH (ENVEO)

ENVIRONMENT CANADA (EC)

FINNISH ENVIRONMENT INSTITUTE (SYKE)

GAMMA REMOTE SENSING RESEARCH AND CONSULTING AG (GAMMA)

NORTHERN RESEARCH INSTITUTE (NORUT)

NORWEGIAN COMPUTING CENTER (NR)

METEOSWISS

UNIVERSITY OF BERN (UNIBE)

CENTRAL INSTITUTE FOR METEOROLOGY AND GEODYNAMICS (ZAMG)

ESA TECHNICAL OFFICER: SIMON PINNOCK

DATE: 8 May 2013

VERSION / REVISION: 1.0 / 02



^b
UNIVERSITÄT
BERN



Schweizerische Eidgenossenschaft
Confédération suisse
Confederazione Svizzera
Confederaziun svizra
Federal Department of Home Affairs FDHA
Federal Office of Meteorology and Climatology MeteoSwiss



This page is intentionally left blank.

DOCUMENT CHANGE LOG

Issue/ Revision	Date	Authors	Checked by	Observations
1.0 / 01	28 Feb 2013	K. Luojus J. Pulliainen J. Lemmetyinen M. Takala C. Derksen		First revision
1.0 / 02	8 May 2013	K. Luojus		Added section 2.3.3 and chapter 4.

This page is intentionally left blank.

Table of Contents

1	Introduction	7
1.1	Purpose of the Document	7
1.2	Structure of the Document	7
1.3	Acronyms	7
1.4	Applicable Documents	8
2	Snow water equivalent algorithm	9
2.1	General overview	9
2.2	Pre-Processing.....	10
2.2.1	Satellite data	10
2.2.2	Weather station data.....	11
2.3	SWE retrieval.....	11
2.3.1	Emission model.....	14
2.3.2	Variable snow density.....	19
2.3.3	Variable snow density based on forest fraction information	22
2.3.4	Cumulative dry snow mask and snow line detection	23
2.3.5	Mountains.....	23
2.4	Aggregated products.....	23
2.5	Auxiliary Data	24
3	Estimation of uncertainty	25
3.1	Consideration of total error for GS SWE product	25
3.2	Spatio-temporal error calculation for SWE product	27
3.2.1	Statistical error of SWE product	27
3.2.2	Absolute, systematic and statistical error levels of SWE product	28
3.2.3	Total spatially and temporally varying error of SWE product	30
4	Conclusions	33
5	References	34

This page is intentionally left blank.

1 INTRODUCTION

1.1 Purpose of the Document

The purpose of this document is to give a detailed description of the algorithms for generating the GlobSnow Snow Water Equivalent (SWE) product. This document presents the algorithm used for producing the diagnostic data set (DDS) of SWE for the GlobSnow-2 project.

1.2 Structure of the Document

Section 2 provides a description of the algorithm for Snow Water Equivalent (SWE) generation. The main retrieval steps are described in detail, including pre-processing, SWE retrieval, emission model and post processing. The algorithm for the actual SWE retrieval is described in Section 2.3. The generation of auxiliary data required as input for SWE mapping is also presented. Retrieval uncertainty is considered in Chapter 3.

1.3 Acronyms

AATSR	Advanced Along-Track Scanning Radiometer (instrument of Envisat)
ATSR	Along-Track Scanning Radiometer (instrument of Envisat)
AVIRIS	Airborne Visible/Infrared Imaging Spectrometer
BEAM	Basic ERS and Envisat (A)ATSR and MERIS Toolbox
CC	Cloud Cover
DDF	Design Definition File
DEM	Digital Elevation Model
ECMWF	European Centre for Middle Range Weather Forecasts
ENVEO	Environmental Earth Observation IT GmbH
ENVISAT	Environmental Satellite of ESA
EO	Earth Observation
EOS	Earth Observing System
ERS	European Remote Sensing Satellite of ESA
ESA	European Space Agency
FCDR	Fundamental Climate Data Record
FMI	Finnish Meteorological Institute
FPS	Full Product Set
FSC	Fractional Snow Cover
MODIS	Moderate Resolution Imaging Spectro-radiometer (instrument of Terra)
MERIS	Medium Resolution Imaging Spectrometer (instrument of Envisat)
NDSI	Normalized Difference Snow Index
NLR	Norwegian Linear Reflectance Algorithm
NR	Norwegian Computing Center
NRT	Near Real Time
OLCI	Ocean and Land Colour Instrument
RMS	Root Mean Square
RMSE	Root Mean Square Error
SAT	Satellite
SCA	Snow Covered Area

SCDA	SYKE's Cloud Detection Algorithm
SCE	Snow Cover Extent
SD	Snow Depth
SE	Snow Extent
SLSTR	Sea and Land Surface Temperature Radiometer
SMAC	Simplified Method for Atmospheric Correction
SoW	Statement of Work
SWE	Snow Water Equivalent
SYKE	Finnish Environment Institute
TOA	Top of Atmosphere
TS	Technical Specification

1.4 Applicable Documents

- [RD-1] EOEP-DUEP-EOPS-SW-08-0006. Statement of Work - DUE *GlobSnow*.
 - [RD-2] GlobSnow Proposal - Technical Annex. Proposed by FMI et al., 2008.
 - [D 1.4] Requirement Baseline Document (RB), GlobSnow team, 2009.
 - [D 1.5] Ground Data Documentation (GDD), GlobSnow team, 2009.
 - [D 1.6] Description of the Diagnostic Data Set (DDS), GlobSnow team, 2009.
 - [D 1.7] Design Justification File, Version 1 (DJF), GlobSnow team, 2009.
 - [D 1.8] Technical Specifications (TS), GlobSnow team, 2009.
 - [D 1.9] Design Justification File, Version 2 (DJF), GlobSnow team, 2009.
 - [D 1.10] Acceptance and Test Document (ATD), GlobSnow team, 2009.
 - [D 1.11] Design Definition File (DDF), GlobSnow team, 2009.
 - [D 1.12] Qualification Review Report (QRR), GlobSnow team, 2009.
 - [D 1.13] Prototype Validation and Assessment Report (PVAR), GlobSnow team, 2009.
 - [D 2.3] Acceptance Review Report (ARR), GlobSnow team, 2010.
 - [D 2.5] Design Justification File 3 (DJF-v3), GlobSnow team 2011
 - [D 2.6] Production and Validation Report (PVR), GlobSnow team, 2011.
 - [D 3.1] Service Evolution Report (SER) v1, GlobSnow team, 2011.
 - [D 3.2] Service Evolution Report (SER-v2) v2, GlobSnow team, 2011.
 - [D 3.5] Final Report (FR), GlobSnow team, 2011.
-
- [RD-3] Statement of Work for GlobSnow-2 EOEP-STRI-EOPS-SW-11-0003, issue 1 revision 0.
 - [RD-4] GlobSnow-2 Consolidated Proposal. Proposed by FMI et al., 2012.

2 SNOW WATER EQUIVALENT ALGORITHM

2.1 General overview

The GlobSnow SWE algorithm combines information from satellite based microwave radiometer and ground based weather station snow depth measurements into hemispherical scale SWE estimates accompanied by uncertainty estimates for each calculation element.

A flowchart of the algorithm on a pixel-level, is presented in Figure 2.1.

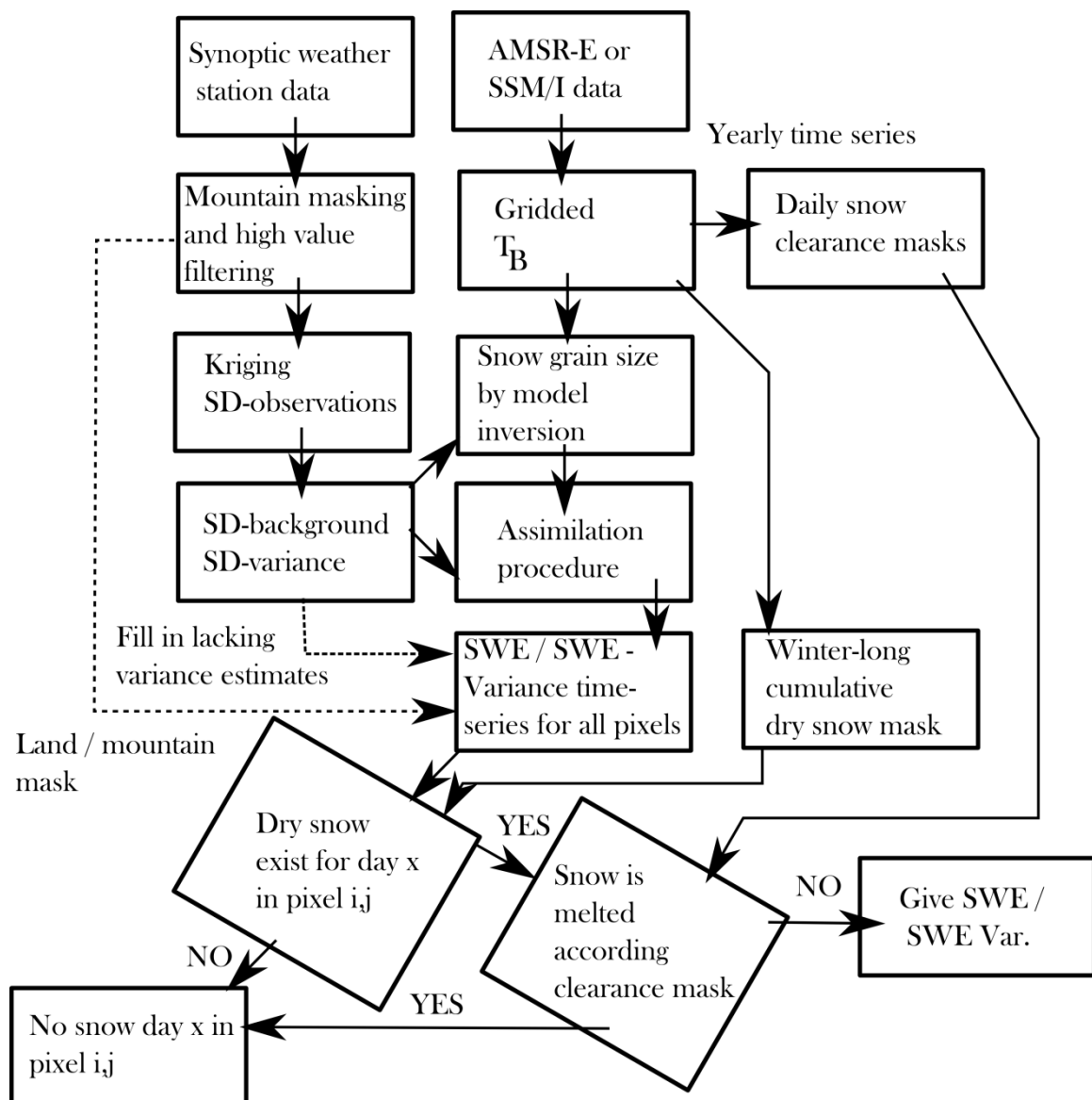


Figure 2.1 The GlobSnow SWE processing chain.

The processing system utilizes satellite data and weather station data, these data and pre-processing steps are described in detail in Section 2.2. The actual retrieval algorithm is presented in detail in Section 2.3. Generation of the aggregated products is presented in Section 2.4. The auxiliary datasets used in SWE retrieval are presented in Section 2.5. The derivation of the SWE variance (uncertainty estimate) is presented in detail in Chapter 3.

2.2 Pre-Processing

The SWE retrieval utilizes spaceborne passive microwave radiometer data and snow depth observations from synoptic weather station. The data acquisition and the pre-processing applied before actual SWE retrieval are presented in this section.

2.2.1 Satellite data

A complete time series of radiometer data from 1978 to present day has been acquired from the National Snow and Ice Data Center (NSIDC) in Boulder, Colorado USA. For the years 1978 to 1987 (July), the Scanning Multichannel Microwave Radiometer (SMMR; Knowles et al., 2002) data from Nimbus 7 are used, whereas for 1987 (August) to present, the Special Sensor Microwave/Imager (SSM/I; Armstrong et al., 1994) data from Defense Meteorological Satellite Program (DMSP) F-08, F-11, F-13 and F-17 are used. There are no adjustments for bias in raw data and thus raw data sets from different satellites are not directly comparable in absolute levels, but include some biases from one instrument to another (a benefit of the SWE mapping methodology applied here is that it reduces the effects of possible biases).

Space-borne observed brightness temperatures (TB) data are in the EASE-Grid north azimuthal equal-area projection with a nominal resolution of 25 km × 25 km (Armstrong et al. 1994). The local overpass time varies in time but the difference between randomly chosen dates is not larger than 2 h. The descending orbit measurements correspond to the early morning (0500 to 0700 local time) and ascending orbit measurements correspond late afternoon (1500 to 1700 local time), although in the case of SSM/I the local overpass time (ascending vs. descending) depends on which DSMP satellite the instrument was onboard. Data used in GlobSnow is a combination of ascending and descending nodes in such way that day-time passes are applied only to the areas where no nighttime passes are available. This enhances the spatial coverage without deteriorating the overall accuracy.

The most important frequencies for snow detection and SWE retrieval are 19 and 37 GHz. Channels close to these frequencies are available from all instruments, although with different native footprint dimensions. These differences in swath level resolution are removed through TB re-sampling to the EASE-Grid as described in (Armstrong et al. 1994). Some data gaps exist both in time and space within the satellite passive microwave data record. SMMR had a narrow swath width (600 km) and was de-activated every other day due to power constraints.

2.2.2 Weather station data

Daily snow depth (SD) background fields were generated from observations at synoptic weather stations acquired from ECMWF for the years 1979 to present (supplemented by INTAS SCCONE data described below). For each measurement, a WMO station identifier, date of measurement, and snow depth (SD) are given. There are no error estimates for the snow depth measurements provided with the ECMWF dataset. The snow depth is traditionally manually measured with a rod or ruler, although in the 1990s there was a transition to automated snow depth sensors in many countries. We account for uncertainty in the point snow depth measurements by assigning a variance of 150 cm² to the observations (based on comparison of point-wise data with coincident snow course measurements from Finland). An unpublished evaluation of point versus transect snow survey measurements from the Environment Canada archive produced a similar variance value.

The ECMWF SD data were enhanced with the inclusion of the INTAS-SCCONE snow depth dataset (Kitaev et al., 2002). This improves the density of surface observations across the former Soviet Union. Manual SD measurements are available for 223 different locations. In addition to information on WMO station identifier, date of measurement and SD, a qualitative estimate of the snow covered area and a status flag value are given. The flag describes whether the observed snow melt was temporary or continuous, and whether the value of SD is correct or should be rejected. The dataset also contains a short description of station characteristics, for example information on whether the station is protected from strong winds or not.

The long-term weather station data is pre-processed before utilization in SWE retrieval to improve the overall representativity of the data.

The synoptic weather station data set is first filtered from extremely large snow depth values (over 300 centimeters, typically occurring only in mountains or extreme locations). Then median filtering is applied to remove values that differ more than 50 cm from the median of 11 days' time frame for each station. After that, stations with at least 20 measurements for at least 5 separate years are kept, the sporadic stations, reporting only for brief time periods are removed. Then stations with unusually deep snow conditions (mean of March over 150 cm) are filtered out if the deep snow conditions have occurred at least 50% of the years that the station has had at least 20 measurements. Lastly snow depth observations above 200 cm are filtered out.

2.3 SWE retrieval

The methodology for SWE retrieval employed by GlobSnow utilizes a Bayesian non-linear iterative assimilation approach first described in Pulliainen (2006) and complemented in Takala et al. (2011). A flowchart of the algorithm is presented in Figure 2.1; there are four primary steps to the retrieval scheme:

Step 1. Snow Depth (SD) observations from synoptic weather stations are obtained for the northern hemisphere from the European Centre for Medium-Range Weather Forecasts (ECMWF; this dataset is described further below). The uncertainty of synoptic SD observations is considered by assigning a variance of 150 cm^2 (a value based on comparison of point-wise synoptic SD data with available coinciding snow survey data sets). The stations located in mountainous areas are filtered out, as are the deepest 1.5 % of reported snow depth values in order to avoid spurious or erroneous deep snow observations. The mountain mask criterion is to remove all observations that fall within Equal Area Scalable Earth Grid (EASE-Grid) cells with a height standard deviation above 200 m within the grid cell. Once this filtering is performed, an ‘*observed SD*’ field is produced from the synoptic weather station observations by ordinary kriging interpolation to the 25 km EASE-Grid. An estimate of the interpolation variance is also obtained. The exponential autocorrelation function of the spatial variability of snow depth is calculated for each day by separately analyzing the observations of North America and Eurasia.

Step 2. The available synoptic weather station measurements of snow depth are used as input to forward model simulations of brightness temperature (T_B) using the multi-layer HUT snow emission model (Pulliainen et al. 1999, Lemmetyinen et al. 2010). The applied version of the model describes the scene brightness temperature as a function of the characteristics of the snow pack (depth, bulk density and grain size) and forest canopy (stem volume/biomass). Additionally, the approach takes into account atmospheric effects to space-borne observed T_B . The model is fit to space-borne observed T_B values at the locations of weather stations by optimizing the value of effective snow grain size. The satellite radiometer measurements are taken from the SMMR and SSM/I sensors. SMMR is used from 1979 to July 1987 and SSM/I from August 1987 to present. The fitting procedure is:

$$\min_{d_0} \left\{ \left(T_{B,19V,mod}(d_0, D_{ref}) - T_{B,37V,mod}(d_0, D_{ref}) \right) - \left(T_{B,19V,obs} - T_{B,37V,obs} \right) \right\}^2 \quad (2.1)$$

where the known snow depth is D_{ref} , $T_{B,19V}$ and $T_{B,37V}$ denote the vertically polarized brightness temperature at approximately 19 and 37 GHz with sub-indices *mod* and *obs* referring to modeled and observed values, respectively. The HUT model describes T_B as a function of SWE, snow density and snow grain size, d_0 in (2.1). A dynamically varying snow density is used, as explained in Section 2.3.2. The observed snow depth at a weather station is used as input to (2.1). At each synoptic station location, the final estimate of the grain size (and its standard deviation λ) is obtained by averaging values obtained for the ensemble of the nearest stations:

$$\langle \hat{d}_{0,ref} \rangle = \frac{1}{M} \sum_{j=1}^M \hat{d}_{0,ref,j} \quad (2.2.a)$$

$$\lambda_{d_{0,ref}} = \sqrt{\frac{1}{M-1} \sum_{j=1}^M \left(\hat{d}_{0,ref,j} - \langle \hat{d}_{0,ref} \rangle \right)^2} \quad (2.2.b)$$

where M is the number of stations (neighbourhood of 6 stations used in GlobSnow). The lower bound for the grain size is set to 0.2 mm with smaller values rounded up.

Step 3. A spatially continuous background field of the effective snow grain size (including a variance field) is interpolated with a kriging technique from the snow grain size estimates produced for the weather station locations in Step 2.

Step 4. A map of spatially continuous ‘*assimilated SWE*’ is produced through forward T_B simulations with the HUT model using the interpolated effective grain size produced through steps (2) and (3) and land cover information (dataset described below). The simulations are compared via a cost function at each grid cell with spaceborne radiometer measurements. The cost function also considers the “*observed SD*” background field. Model estimates are matched to observations numerically by fluctuating the SWE value. The cost function constrains the grain size value according to the predicted background grain size and the estimated variance produced in Step 3. Thus, assimilation adaptively weighs the space-borne brightness temperature observations and the ‘*observed SD*’ field (produced in step 1) to estimate a final SWE and a measure of statistical uncertainty (in the form of a variance estimate) on a grid cell by grid cell basis:

$$\min_{D_t} \left\{ \left(\frac{(T_{B,19V,mod}(D_t) - T_{B,37V,mod}(D_t)) - (T_{B,19V,obs} - T_{B,37V,obs})}{\sigma_t} \right)^2 + \left(\frac{D_t - \hat{D}_{ref,t}}{\lambda_{D,ref,t}} \right)^2 \right\} \quad (2.3)$$

where $\hat{D}_{ref,t}$ is the snow depth estimate from the kriging interpolation for the day under consideration, t in (2.3). $\lambda_{D,ref}$ the estimate of standard deviation from the kriging interpolation, and D_t is the snow depth for which equation (2.3) is minimized (note that $D_t = SWE/snow\ density$). The variance of the T_B is σ_t . It can be estimated by approximating T_B (a function of snow depth and grain size) by a Taylor series:

$$T_B(D_t, d_0) \approx T_B(D_t, \langle \hat{d}_{0,ref,t} \rangle) + \frac{\partial T_B(D_t, \langle \hat{d}_{0,ref,t} \rangle)}{\partial d_0} (d_0 - \langle \hat{d}_{0,ref,t} \rangle) \quad (2.4.a)$$

$$\sigma_t^2 = \text{var}(T_B(D_t, \langle \hat{d}_{0,ref,t} \rangle)) = \left(\frac{\partial T_B(D_t, \langle \hat{d}_{0,ref,t} \rangle)}{\partial d_0} \right)^2 \lambda_{d0,ref,t}^2 \quad (2.4.b)$$

The variance σ_t^2 in (2.3) and (2.4) is a parameter that adjusts the weight of brightness temperature data with respect to the weight of the ‘*observed SD*’ field (parameter $\lambda_{D,ref}$). A basic feature of the algorithm is that if the sensitivity of space-borne radiometer observations to SWE is assessed to be close to zero by formulas (2.4.a) and (2.4.b), the weight of radiometer data on producing the ‘*assimilated SWE*’ approaches zero (this is the case e.g. if the magnitude of SWE

is very high). The higher is the estimated sensitivity of T_B to SWE, the higher is the weight given to the radiometer data. Thus, the weight of the radiometer data varies both temporally and spatially in order to provide a maximum likelihood estimate of SWE.

A comparison of point-wise ECMWF SD-observations with areally distributed snow surveys (INTAS-SCONE data set covering Russian and Finnish snow courses has indicated a random difference with a variance level of about 100 - 150 cm². Thus, a variance of 150 cm² is attributed to SD measurements at the location of weather stations (this is also considered by $\lambda_{D,ref}$ in (2.3)). While it is possible to use previous SWE estimates in the assimilation algorithm (Pulliainen, 2006), currently in GlobSnow the SWE is estimated on a per day basis with no consideration of previous retrievals.

2.3.1 Emission model

The snow emission model applied is the improved multi-layer semi-empirical HUT snow emission model, consisting of the original model by (Pulliainen et al. 1999) and an expansion to multiple layers by (Lemmetyinen et al. 2010), both briefly explained below.

The original HUT snow emission model (Pulliainen et al., 1999) is a radiative transfer-based, semi-empirical model which calculates the emission from a single homogenous snowpack. A delta-Eddington approximation is used in the radiative transfer equation, applying an empirical constant to determine the forward scattered intensity of snow. The extinction coefficient of snow, dependant on snow grain size and frequency, is calculated empirically according to Hallikainen et al. (1987). Snow wetness and salinity content can be simulated if required; the dielectric constant for wet snow is described through an empirical formula. Reflection and transmission coefficients and the refraction angle between layer interfaces are calculated using an incoherent approach (Ulaby et al., 1981) following Fresnel's law. Scattering effects due to ground surface roughness are calculated according to Wegmüller and Matzler (1999). Additionally, separate empirical or statistical modules account for the influence of the surface vegetation (Kruopis et al., 1999) and atmospheric effects.

The original HUT snow emission model calculates the emission from a single homogenous snowpack using a two-flux approximation. Input parameters of the model include snowpack depth, density, effective grain size and temperature. Snow moisture content and snow (or ice) salinity can be included by modifying the dielectric constant through empirical equations.

For radiation propagating in a snowpack at depth d' in angle θ , the radiative transfer equation can be expressed as (Pulliainen et al., 1999):

$$\begin{aligned} \frac{\partial T_B(d', \theta)}{\partial d'} &= \kappa_a \sec \theta T_S \\ &+ \kappa_s \sec \theta \frac{1}{4\pi} \iint_{4\pi} \Psi(\bar{r}_\theta, \theta', \phi') T_B(d', \theta', \phi') \sin \theta' d\theta' d\phi', \\ &- \kappa_e \sec \theta T_B(d', \theta) \end{aligned} \quad (2.5)$$

Where T_B is the brightness temperature, T_S the physical snow temperature, κ_a the absorption coefficient, κ_e the extinction coefficient, κ_s the scattering coefficient, Ψ the scattering phase function and \bar{r}_θ the unit vector to the angle of observation.

The HUT model assumes that most scattering of radiation propagating in a snowpack is concentrated in the forward direction (of propagation). This assumption is based on previous studies by Hallikainen et al. (1987); similar results have been obtained using a theoretical model (Tsang et al., 2007). The HUT model applies the delta-Eddington approximation to the radiative transfer equation; In the case of dominant forward scattering, the scattered incoherent intensity for a thin snowpack of thickness d can be expressed as (Ishimaru, 1978):

$$I_{inc} = I(0^+) q [e^{-\kappa_a d} - e^{-\kappa_e d}] \quad (2.6)$$

where q is a constant describing the fraction of radiation scattered in the forward direction through multiple scattering effects. Assuming this to be valid simplifies the radiative transfer equation to

$$\frac{\partial T_B(d', \theta)}{\partial d'} = \kappa_a \sec \theta T_S + \sec \theta (q\kappa_s - \kappa_e) T_B(d', \theta), \quad (2.7)$$

The emission of a medium with thickness d_0 just below the medium boundary can be then obtained from (Pulliainen et al., 1999):

$$\begin{aligned} T_{SNOW} &= T_0 \frac{\kappa_a}{\kappa_e - q\kappa_s} \left(1 - \frac{1}{L}\right) \\ &= T_s \frac{\kappa_a}{\kappa_e - q\kappa_s} (1 - \exp((- \kappa_e + q\kappa_s) \cdot d_0 \cdot \sec \theta)) \end{aligned} \quad (2.8)$$

where $1/L$ is the attenuation.

An empirical equation is used to relate the snow extinction coefficient to frequency and snow grain size (Hallikainen et al., 1987), so that for frequencies 1 to 60 GHz

$$\kappa_e = 0.0018 f^{2.8} D_{obs}^2. \quad (2.9)$$

Where f is the frequency in GHz and D_{obs} is the observed scattering particle (snow grain) diameter in millimeters.

The empirical parameter q has been defined for snow by fitting the HUT model to experimental snow slab emission data (Pulliainen et al., 1999). The emission data, presented by Weise (1996), represents several snow types and spans a frequency range from 11 to 94 GHz. A common value of $q=0.96$ was found to be applicable for all frequencies in this range (Pulliainen, 1999).

It should be noted that the parameter q includes effects from multiple scattering in the snowpack, and is as such relatively high compared to a case of singular scattering following e.g. the Mie theory. As pointed out by Hallikainen et al. (1987), in snow the losses due to scattering are approximately equal to generation of incoherent intensity by scattering. This is supported also by recent theoretical studies of multiple scattering in snow, which predict that on microwave frequencies, the largest part of total volume scattering to be in the forward direction (Tsang et al., 2007).

The absorption coefficient κ_a is determined from the complex dielectric constant of dry snow, applying the Polder-van Santen mixing model for the imaginary part (Hallikainen et al., 1986). The calculation of the real part of the dielectric constant for dry snow is presented by Mätzler (1987). Reflection and transmission coefficients and the refraction angle at layer interfaces are calculated following the Fresnel equations. Emission from the snow layer is considered as both up-and downwelling emission. These are, in turn, reflected from interfaces between layers (air-snow, snow-ground). The transmission and multiple reflections between layers interfaces are calculated using the incoherent power transfer approach presented by Ulaby (1981).

For emission from a layer consisting of pure ice, it is assumed that $q=1$ and thus $\kappa_a = \kappa_e - q\kappa_s$, corresponding to a non-scattering absorbing layer, simplifying (2.8) to

$$T_{ICE} = T_{phys} (1 - \exp((- \kappa_a) \cdot d_0 \cdot \sec \theta)). \quad (2.10)$$

The determination of grain size from observations has traditionally proved problematic; an empirical formula to relate observed grain size to an effective grain size suitable for the HUT snow emission model has been proposed by Kontu and Pulliainen (2010). The formula reduces the effect of variations and large values in observed grain size. According to the study, the effective grain size D_{eff} , i.e. the grain size value that corresponds to the total scattering effects from the snowpack, can be related to observations by

$$D_{eff} = 1.5 \cdot (1 - \exp(-1.5 \cdot D_{obs})). \quad (2.11)$$

The equation 2.11 is currently not applied in the emission model within GlobSnow, but is still being investigated as a possible improvement. The merit of (2.11) on hemispherical scale is not yet sufficiently known.

A recent expansion to the HUT snow emission model allows for the inclusion of multiple layers in the simulation (Lemmetyinen et al., 2010). The treatment of multiple layers is based on a two-flux approximation of each layer (Ishimaru, 1978). Layers are considered infinite in the horizontal direction.

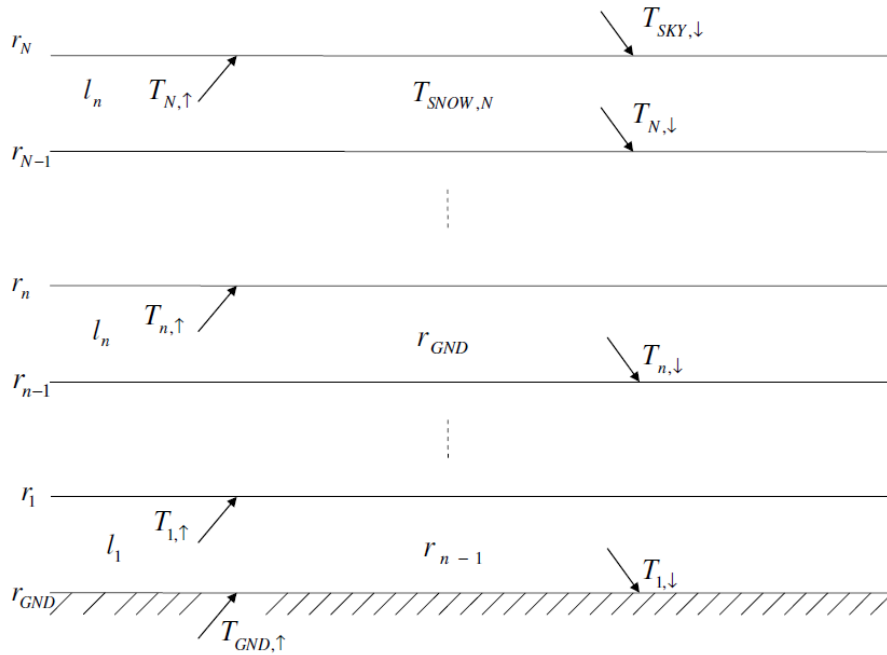


Figure 2.2: Schematic overview of the new multiple layer HUT snow emission model, with N -layers of snow or ice, each with brightness temperature $T_{SNOW,n}$, reflection r_n and attenuation l_n . Air and ground layers (layers $N+1$ and “0”, respectively) contribute their respective up- and downwelling brightness temperatures T_{SKY} and T_{GND} to the system (from Lemmetyinen et al, 2010).

Only incoherent power transfer is considered. Layer interfaces between consecutive snow layers, and the topmost air-snow interface, are considered. The upwelling emission flux $T_{n,\uparrow}$ of layer n of a system as depicted in Figure 2.2 can be determined as

$$T_{n,\uparrow} = S_n \left(T_{SNOW,n} + T_{n+1,\downarrow} \frac{t_n \cdot r_{n-1}}{l_n^2} + T_{n-1,\uparrow} \frac{t_{n-1}}{l_n} + T_{SNOW,n} \frac{r_{n-1}}{l_n} \right), \quad (2.12)$$

where t_n , r_n and l_n are the Fresnel transmission and reflection coefficients, and the loss factor of layer n , respectively. S_n is the geometric sum of multiple reflections in layer n .

Similarly, the downwelling emission is:

$$T_{n,\downarrow} = S_n \left(T_{SNOW,n} + T_{n+1,\downarrow} \frac{t_n}{l_n} + T_{n-1,\uparrow} \frac{t_{n-1} \cdot r_n}{l_n^2} + T_{SNOW,n} \frac{r_n}{l_n} \right). \quad (2.13)$$

By considering the up- and downwelling fluxes of each layer, the total upwelling emission $T_{N,\uparrow}$ beneath the topmost layer is solved. The observed emission from above the snowpack when multiplied by $t_N = (1 - r_N)$. The multiple layer adaptation can also be directly employed in the simulation of a water-ice-snow system, such as snow covered lake ice.

The HUT model includes a simple empirical module for compensation of effects of vegetation. The total scenery can be modified by the fractional amount of vegetation in the observation, so that for the vegetated part the brightness temperature is given as

$$T_{B,for} = \left[1 - \frac{1}{L_c} (1 - e_{snow}) \right] T_s, \quad (2.14)$$

Where T_s is the physical temperature, L_{can} is the canopy cover loss factor and e_{snow} the emissivity of snow covered ground. The loss factor L_{can} is obtained from the empirical forest transmissivity model by Kruopis et al. (1999). The total brightness temperature of a "scenery" can then be summed from several components, divided e.g. by land cover type (dense/sparse forest, field, etc) so that

$$T_B^{tot} = \sum_{\mu=1}^M \beta_{\mu} T_{B,\mu}^i, \quad (2.15)$$

where β_{μ} is the fractional (0...1) coverage and $T_{B,\mu}^i$ the brightness temperature originating

from of land cover type μ , so that $\sum_{\mu=1}^N \beta_{\mu} = 1$.

The vegetation transmissivity model is based on airborne measurements of snow-covered forest in Oulu and Sodankylä areas, Finland. Measurements near Oulu were made on 6.8, 10.65, and 18.7 GHz and both V and H polarizations. Measurements near Sodankylä used 24, 34, 48, and 94 GHz but only V polarization. The final model used here is based on the measurements on V

polarization only. The model calculates the transmissivity t of the vegetation using stem volume V (m³/ha):

$$t(f, V) = t(f, V_{high}) + [1 - t(f, V_{high})] \cdot e^{-0.035V}, \quad (2.16)$$

where

$$t(f, V_{high}) = 0.42 + (1 - 0.42) \cdot e^{-0.028f}. \quad (2.17)$$

Atmospheric effects are modelled using measurements near the ground with a statistical atmospheric model (Pulliainen et al., 1993). In the statistical model, the upwelling brightness temperature of the atmosphere is calculated with:

$$T_{atm,\uparrow} = \alpha_{\uparrow} \cdot T_{\Omega} \cdot (1 - \tau), \quad (2.18)$$

where α_{\uparrow} is the approximate atmospheric profile factor, T_{Ω} is the surface (air) temperature (K) and τ is the atmospheric transmissivity derived from statistical studies (Salonen et al., 1990). Downwelling brightness temperature is calculated analogous to equation (2.14). Since the statistical model assumes average conditions, there are always some clouds included. The input parameters to the physical model are temperature, pressure and absolute humidity. The physical model is able to calculate the effects of clouds, if there are enough input data of cloud properties.

2.3.2 Variable snow density

Much of the GlobSnow SWE retrieval processing is actually based on snow depth information because this is the variable directly measured at climate stations across the northern hemisphere (for instance, see equations 2.2a, 2.2b, 2.3, 2.4a, 2.4b). At a given point, snow depth (h_s) is related to SWE by the local bulk density (r_b):

$$SWE = h_s \times (r_b/r_w) \quad (2.21)$$

where depth is measured in centimeters, density in grams per centimeters cubed, r_w is the density of water (1 g cm⁻³), and SWE is measured in centimeters of water.

To convert from depth to SWE, inferences about the snow density must be made because of the lack of density measurements across much of the northern hemisphere. The first implementation of the GlobSnow SWE retrieval scheme utilized a fixed density of 0.240 g/cm³ regardless of snow depth, location, or time of year. While these assumptions are not realistic, analysis of large coincident datasets of depth, density, and SWE show that depth varies over a

range that is many times greater than the range of bulk density (Sturm et al., 2010). Using a fixed conservative parameter (r_b) while directly working with the more dynamic (and easier to measure) parameter (h_s) was a reasonable decision. Implementing a spatially and temporally dynamic treatment of snow density, however, is more physically sound and should improve the SWE retrievals particularly during the shoulder seasons when snow density is less (fall) and greater (spring) than 0.240 g/cm^3 .

A number of options of varying complexity were considered for the implementation of variable snow density in GlobSnow-2. Each option first required the segmentation of the northern hemisphere into climatological snow classes, following Sturm et al. (1995; see Figure 2.3). If mean snow density from the Brown and Mote (2009) climatology is then assigned to each snow class, it is clear that the fixed density of 0.240 g/cm^3 using in GlobSnow-1 results in systematic underestimation of SWE in the conversion from snow depth for all snow classes except taiga (Figure 2.4).

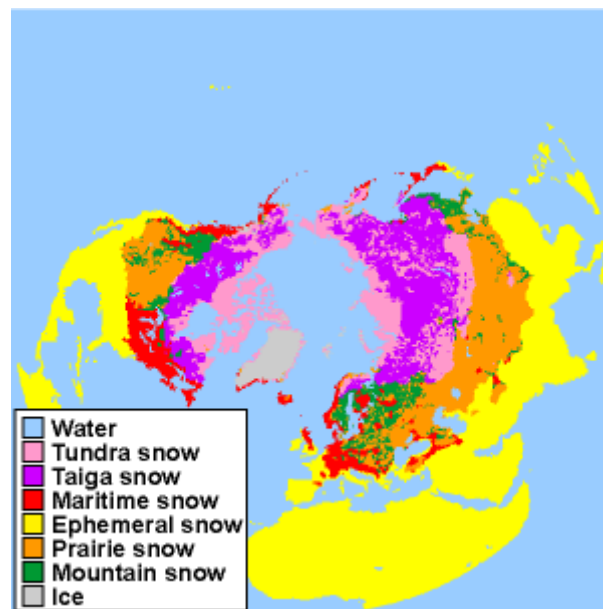


Figure 2.3. Climatological snow classes for the Northern Hemisphere as defined by Sturm et al. (1995).

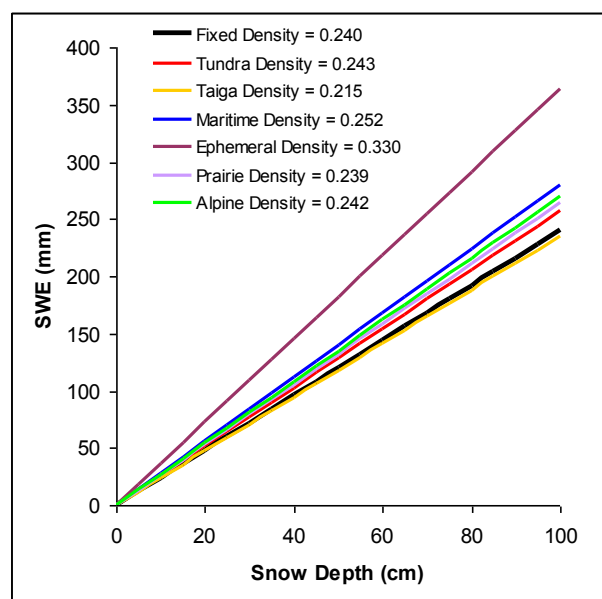


Figure 2.4 Snow depth versus SWE relationships using fixed densities by snow class.

While use of this simple approach would still represent improvement over a static snow density, fully dynamic spatial and temporal treatment of density within GlobSnow-2 will utilize a statistical model based on a Bayesian analysis of coincident depth–density–SWE data as presented in Sturm et al. (2010). If depth, day of year, and snow climate class are specified for a given location (all of which are known in the GlobSnow retrieval), a local bulk density estimate can be produced:

$$\rho_{hi,DOY_i} = (\rho_{max} - \rho_0)[1 - \exp(-k_1 \times h_i - k_2 \times DOY_i)] + \rho_0 \quad (2.22)$$

where k_1 and k_2 are densification parameters for depth and DOY, respectively; ρ_{max} , ρ_0 , k_1 , and k_2 vary with snow class (Table 2.1); and i indicates the i th observation. Because the winter season in the northern hemisphere spans two calendar years, DOY runs from -92 (1 October) to +181 (30 June), with no 0 value.

Table 2.1 Model parameters by snow class for determining density (from Sturm et al., 2010).

Snow class	ρ_{max}	ρ_0	k_1	k_2
Alpine	0.5975	0.2237	0.0012	0.0038
Maritime	0.5979	0.2578	0.0010	0.0038
Prairie	0.5940	0.2332	0.0016	0.0031
Tundra	0.3630	0.2425	0.0029	0.0049
Taiga	0.5000	0.2170	0.0000	0.0000

Determining the appropriate density to convert snow depth to SWE within the GlobSnow scheme therefore only requires a static mask of snow cover class, the final daily snow depth estimates from the retrieval system, the day of year, and the coefficients provided in Table 2.1. Sensitivity analysis of the impact of variable snow density using this approach for a fixed snow depth of 50 cm is shown in Figure 2.5. The snow density for all snow classes increases through

the snow season, with the rate of this increase dependent on snow class. Note the density for taiga remains constant as the seasonal evolution of density is very limited for this snow class (the k_1 and k_2 coefficients are 0). The overall impact of the transition to a variable density within the GlobSnow retrieval scheme will be evaluated using independent reference measurements.

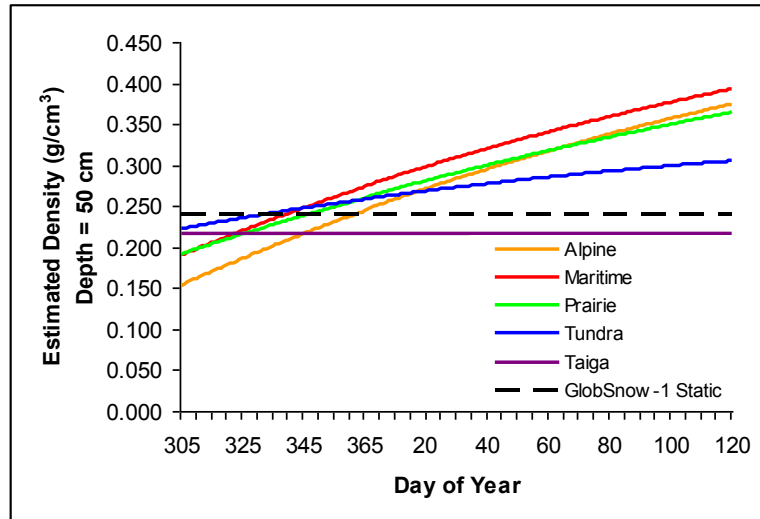


Figure 2.5. Estimated snow density through the snow season using Sturm et al. (2010) equation 6 for a fixed snow depth of 50 cm.

2.3.3 Variable snow density based on forest fraction information

The baseline approach (section 2.3.2) for variable snow density leads into very distinct borders in SWE retrieval between adjacent pixels that are from different snow classes. In order to mitigate this issue, it was decided to weigh the snow density of each pixel, based on the amount of forest within that pixel.

The modified snow density approach calculates the final snow density for each pixel by weighing the snow densities calculated by equation (2.22) with the amount of forest within the pixel, using the following equation:

$$\rho_{\text{final}} = (ff * \rho_{\text{taiga}}) + ((1 - ff) * (\rho_{\text{prairie}} + \rho_{\text{tundra}}) / 2) \quad (2.23)$$

where ρ_{final} is the final snow density for the pixel, ff is the fraction of forest for the pixel, ρ_{taiga} , ρ_{prairie} and ρ_{tundra} are the snow densities for taiga, prairie and tundra respectively, each calculated using the Sturm et al. approach (equation 2.22).

The forest fraction is determined from the ESA DUE GlobCover data.

2.3.4 Cumulative dry snow mask and snow line detection

In order to provide a hemispheric SWE map for the region of seasonal snow cover, it is also necessary to produce a cumulative dry snow mask for each snow cover season (beginning September 1). For this purpose, the dry snow detection algorithm of Hall et al. (2002) is applied to satellite radiometer data. From satellite passive microwave measurements, the date of snow clearance can also be estimated using the algorithm of Takala et al. (2009). If the cumulative dry snow mask shows that a grid cell in question for a particular date has never been marked as dry snow it is labeled as snow free through the winter. If the cumulative dry snow mask suggests that the pixel has had dry snow conditions, but is already snow free according to the snow clearance algorithm, the pixel is marked as snow free. An estimate of the SWE and SWE variance are given for grid cells for which dry snow cover has been detected and for which snow melt has not yet been indicated.

SWE estimates for wet snow areas (where retrieval using the radiometer data is not feasible) are determined from the weather station data using kriging interpolation (for wet snow cover the algorithm inherently assesses the weight of radiometer data to approach zero).

The areas that are identified as snow covered with the melt detection algorithm, but for which a SWE estimate is not produced, are given a marginal SWE value (0.001 mm) in the final SWE product. This information can be used to determine the extent of snow cover. The areas with a SWE value of 0 mm are bare ground, and areas with SWE of 0.001 mm or above are snow covered these determine the snow line for the SWE product.

The relation between the SWE and snow cover extent is:

- 0 [mm] -> snow-free areas (Snow Extent 0%)
- 0.001 [mm] -> areas with melting snow (Snow Extent between 0% - 100%)
- >0.001 [mm] -> areas with full snow cover (Snow Extent 100%)

2.3.5 Mountains

If a grid cell is in mountainous areas it is flagged as such and no SWE is retrieved due to the uncertainty of microwave measurements in complex, snow covered Alpine terrain. Topographic information for the masking of complex terrain is derived from ETOPO5 (National Geophysical Data, 1988) data. Within GlobSnow, an EASE-Grid cell is considered as mountainous if the standard deviation of the elevation within a grid cell is above 200m.

2.4 Aggregated products

There are three products derived for SWE, a baseline daily product and two aggregated products:

- **Daily Snow Water Equivalent** (Daily L3A SWE), snow water equivalent (mm) for each grid cell for all evaluated land areas of the Northern Hemisphere.

- **Weekly Aggregated Snow Water Equivalent** (Weekly L3B SWE), calculated for each day based on a 7-day sliding time window aggregation of the daily SWE product.
- **Monthly Aggregated Snow Water Equivalent** (Monthly L3B SWE) a single product for each calendar month providing the average and maximum SWE, calculated from the daily and weekly aggregated SWE products.

The weekly (7-days) aggregated product is calculated using sliding window averaging: the SWE estimate for the current day is calculated as a mean of the samples from the previous 6 days and the current day SWE (for each grid cell). The monthly aggregate, a single product for each calendar month, is calculated by determining the mean from the daily SWE products and the maximum from the weekly SWE products. Using the weekly data to derive the maximum for the monthly product reduces the possible effect of a single unrealistically high daily SWE value to directly translate to the level of the maximum monthly SWE.

2.5 Auxiliary Data

The SWE retrieval utilizes information on land cover, forest biomass, water bodies and distinction between mountainous and non-mountainous regions.

The Global Land Cover 2000 is used as land use information for the assimilation algorithm (<http://bioval.jrc.ec.europa.eu/products/glc2000/glc2000.php>). The dataset covers the whole globe at a resolution of 1 km with 23 land cover classes. Areal fractions of two basic land cover categories are calculated for each EASE-Grid cell and used as input to the forward Tb model in the assimilation scheme. The two applied land cover classes are (a) forest and (b) all other land cover classes. Grid cells with major lakes are masked out if the areal fraction of open water exceeds 50%. The approximate forest biomass (stem volume) is assigned to the forest fraction of each grid cell. For North America, a mean forest stem volume value of 80 m³/ha is used to characterize the effect of forest cover based on FAO statistics (<http://www.fao.org/forestry/32042/en/>). While this is a very generalized approach, estimation of effective grain size greatly reduces the sensitivity of the algorithm to forest biomass allowing a constant value to be adopted. For northern Eurasia, a spatially varying stem volume value is assigned to the forest fraction of each grid cell based on a digital forest map described in Bartalev et al. (2004).

Topographic information for the masking of complex terrain is derived from ETOPO5 (National Geophysical Data, 1988) data. This dataset contains global elevation information at a resolution of 5 arc minutes, an appropriate resolution given the scale of the 25 km EASE-Grid. Within GlobSnow, an EASE-Grid cell is considered as mountainous if the standard deviation of the elevation within a grid cell is above 200m.

3 ESTIMATION OF UNCERTAINTY

3.1 Consideration of total error for GS SWE product

The total residual error in SWE product is composed of two contributions (a) statistical random error and (b) systematic error. Statistical error is here defined as a theoretical error that can be estimated through an error propagation analysis. Presently, the GS SWE product calculates this error contribution through an adaptive formulation that takes into account both spatially and temporally varying characteristics of the applied input data (Pulliainen, 2006; Takala et al., 2011). That is, the accuracy characteristics of applied space-borne microwave radiometer observations and those of weather-station observed snow depth information. In particular, the dynamic sensitivity of microwave radiometer observations to SWE is considered.

The systematic error can be understood to include all unknown error factors that may also vary both spatially and fluctuate temporally. Typically, the inaccuracy of forward modeling can include such deficiencies that result to biases in the outcome of inversion algorithms (geophysical retrievals). Thus, the magnitude of systematic error can be only evaluated through comparison with (independent) validation data, which may include both regional and temporal aspects. For example the biases of snow retrieval algorithms can be different for different snow regimes and they may show variability between different seasons and from one winter to another.

The starting point of the calculation procedure for a spatially and temporally varying total residual error is the consideration of regional or global error (for the period under investigation):

$$RMSE_{abs} = \sqrt{\frac{1}{N} \sum (RMSE_{stat}(x, y, t))^2 + \Delta^2} \quad (3.1)$$

where $RMSE_{abs}$ is the total error level that can be estimated through the comparison of SWE/SE estimates with independent reference data (for the region and time-period under investigation). $RMSE_{stat}$ is the modeled statistical error obtained through error propagation analysis. It may vary spatially over locations (x,y) and moments of time (t) with a total number of cases N . The remaining (systematic) error contribution is a scalar that is assumed to be independent on the statistical error and it is here denoted by Δ .

Thus, Δ can be obtained by:

$$\Delta = \sqrt{RMSE_{abs}^2 - \frac{1}{N} \sum (RMSE_{stat}(x, y, t))^2} \quad (3.2)$$

Hence formula (3.2) gives an estimate of the level of error contribution that cannot be explained by the statistical random error.

After Δ is determined through the analysis of reference data set, the pixel-wise time-dependent error of the SWE/SE product is directly obtained by:

$$RMSE_{tot}(x, y, t) = \sqrt{\Delta^2 + (RMSE_{stat}(x, y, t))^2} \quad (3.3)$$

The implementation of (3.2) – (3.3) to SWE product line includes the consideration of Δ in a global scale by analyzing all available reference data as a single data set. Alternatively, the reference can be divided regionally or temporally. This is in practice dependent upon the availability of independent validation data. As a summary, Figure 3.1 shows the flowchart of the process for the estimation of the total product error.

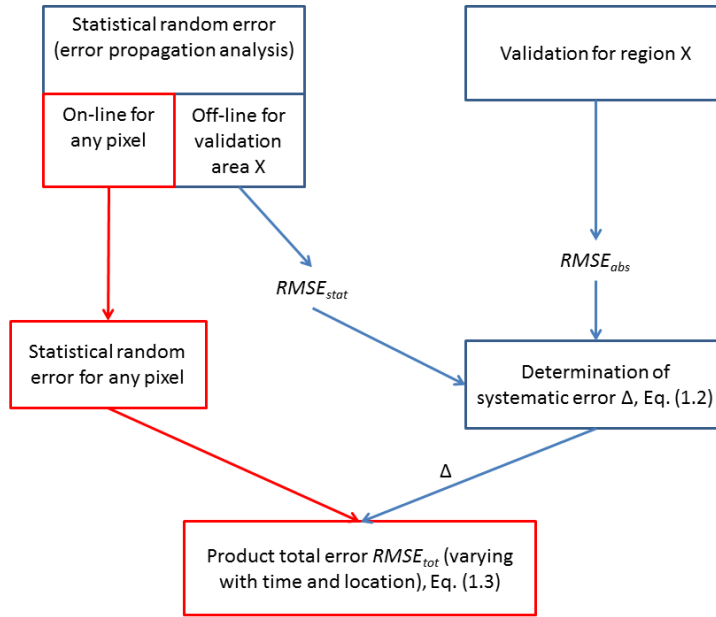


Figure 3.1. Procedure for the on-line determination of the product total error (SWE or fractional snow cover area, FSC). The calculation of systematic error is performed off-line with validation data set.

One should also notice that a bias correction to the retrieval results can be through an analogous analysis. First, the bias is obtained by:

$$BIAS = \frac{1}{N} \sum_{i=1}^N (\hat{Y}_i - Y_i) \quad (3.4)$$

where Y_i is the ground truth observation for the point i and \hat{Y}_i is the estimate for the variable by the inversion algorithm. Thus, the bias-corrected estimate is simply:

$$\hat{Y}_{i,BIAScorr} = \hat{Y}_i - BIAS \quad (3.5)$$

3.2 Spatio-temporal error calculation for SWE product

3.2.1 Statistical error of SWE product

The algorithm for SWE estimation is based on the variational data assimilation combining information from synoptic weather stations and passive microwave radiometers. The method considers the accuracy characteristics of both information sources and determines the spatially and temporally varying variance of uncertainty for the SWE estimates.

The algorithm input from synoptic weather stations is the point-wise snow depth observation. An essential factor influencing the SWE estimate is the error variance assigned to this observation. This variance should explain how well the single-point observation corresponds to the areally distributed value in a satellite footprint (having a size of e.g. 25 km × 25 km). Based on the comparison of ECMWF-database-derived snow depth (SD) data with Russian INTAS-SCCONE snow course data, this variance has been found to range from 100 to 150 cm², i.e. standard deviation ranges from 10.0 to 12.2 cm, (Takala et al., 2011). Thereby, GlobSnow product versions 1.0, 1.2 and 1.3 have applied a constant value of 150 cm² to describe the snow depth observation error variance.

A recent investigation with Finnish data representing boreal forest zone has indicated a RMSE difference of 10.1 cm when comparing weather station observations of snow depth with distributed observations from snow courses (Metsämäki et al., 2012). The multi-year Canadian *in situ* data from intensive tundra field campaigns near Daring Lake, NT, indicates a much higher spatial variability for tundra regions, see e.g. Takala et al. 2011. According to these data, a standard deviation of 20 cm is a feasible value for the sub-pixel snow depth variability. Thus, this value can be assigned to represent the uncertainty of weather station observed snow depth at tundra regions. This value is also reasonable for prairie/steppe regions, since according to some investigations (e.g. Liston 2004), the sub-pixel variability SWE at prairie regions may be even larger than in tundra.

In addition to the uncertainty of weather station observed SD, the statistical error is affected by the estimated uncertainty of the (forward) modeling of space-borne observed brightness temperature (T_B) and the estimated sensitivity of T_B to SWE. The concept of statistical error in SWE retrieval is summarized by the following equations. The basic formula for the variance of the uncertainty of the SWE estimate, at the location under investigation and moment of time (t), is given by:

$$\text{var}(SWE_t) = \text{var}(\rho_{snow} D_t) = \rho_{snow}^2 \text{var}(D_t) = \rho_{snow}^2 \left[\frac{1}{\left(\frac{\partial T_{B,t}}{\partial D} \right)^2 \sigma_t^2 + \sigma_{REF,t}^2} \right] \quad (3.6)$$

where

ρ_{snow} = snow bulk density,

D_t = snow depth (at the moment of time t),

σ = uncertainty of forward modeling (standard deviation of the modeling error)

σ_{REF}^2 = variance of the (spatial) uncertainty of weather station-observed snow depth.

Further on, the uncertainty of the forward modeling required for (1) is calculated by:

$$\sigma_t^2 = \text{var} \left(T_B(D_t, \langle \hat{d}_{0,ref,t} \rangle) \right) = \left(\frac{\partial T_B(D_t, \langle \hat{d}_{0,ref,t} \rangle)}{\partial d_0} \right)^2 \lambda_{d_{0,ref,t}}^2 \quad (3.7)$$

where

D = snow depth,

$\langle \hat{d}_{0,ref,t} \rangle$ = estimated block-averaged snow grain size,

d_0 = snow grain size,

$\lambda_{d_{0,ref,t}}$ = estimated standard deviation of block averaged snow grain size (for the location under investigation and the moment of time t).

The current SWE algorithm implementation determines $\hat{d}_{0,ref,t}$ for each individual weather station by fitting the forward model of T_B to observations. Then, the ensemble estimates are calculated (again for each station) from the observations of the 6 closest-by weather stations:

$$\langle \hat{d}_{0,ref} \rangle = \frac{1}{M} \sum_{j=1}^M \hat{d}_{0,ref,j} \quad (3.8)$$

and

$$\lambda_{d_{0,ref}} = \sqrt{\frac{1}{M-1} \sum_{j=1}^M (\hat{d}_{0,ref,j} - \langle \hat{d}_{0,ref} \rangle)^2} \quad (3.9)$$

The standard deviation of grain, estimated for each applied weather station, is interpolated to cover all pixels of the SWE mapping area. However, the next product version will estimate the grain size information for each calculation grid cell based on the interpolated weather station-observed SD. Then the block averaging is carried out for a fixed window size independently from the density of weather stations.

3.2.2 Absolute, systematic and statistical error levels of SWE product

The absolute error level of SWE product can be estimated using two data sets: the INTAS-SCCONE snow course data on SWE for Russia and former Soviet Union and the Finnish snow course observation data set. These data facilitate the analysis of absolute error as a function of SWE, for different years and for different land cover categories or climate zones. According to these data the overall error level of GlobSnow SWE product version 1.2 is 49.3 mm. However, this error is strongly affected by the level of SWE. Figure 3.2 depicts the absolute accuracy of SWE product as a function of SWE based on the analysis of 147207 INTAS-SCCONE reference observations on SWE for a period of 30 years. The estimated contributions of systematic error and statistical error are also shown based on (3.1) – (3.3), and they are calculated separately for 5 SWE categories: 0 mm <SWE ≤ 50 mm, 50 mm <SWE ≤ 100 mm, 100 mm <SWE ≤ 150 mm, 150

mm <SWE ≤ 200 mm and 200 mm < SWE. Figure 3.2 also shows the exponential fit to discrete class-wise estimates of systematic error. Note that the statistical error is the RMS-value of the pixel-wise error:

$$\langle RMSE_{stat} \rangle = \sqrt{\frac{1}{N} \sum (RMSE_{stat}(x, y, t))^2} \quad (3.10)$$

In (3.10) and Figure (3.2), N is the number of all samples for a certain SWE category. However, the actual revised error of the GlobSnow ver.1.3 SWE product has to be determined as a function of estimated SWE. This is shown in Figure 3.3. Again, an exponential fit can be applied to approximately describe the behavior of systematic error as a function of SWE. The obtained fitting curve is:

$$\Delta = 17.25 \exp(0.0058 \text{ SWE}) \quad (3.11)$$

This function gives the systematic error as function of SWE, even though as shown by Figure 3.3, the observed systematic error differs relatively much from the fitting curve for the lowest level of SWE. This evidently occurs due to inaccuracies in snow free surface detection.

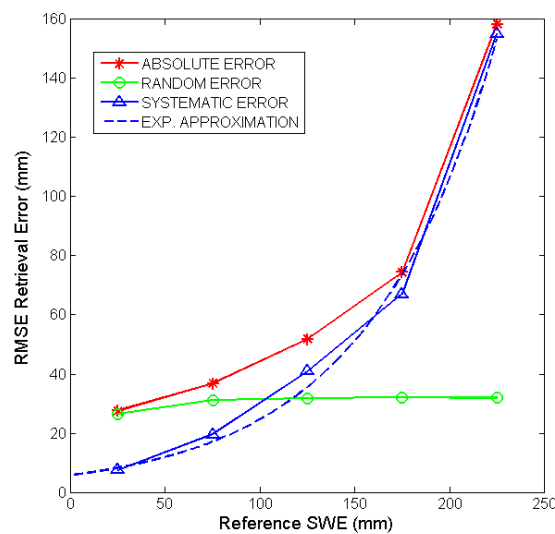


Figure 3.2. Total error of GlobSnow ver.1.3 SWE product with different levels of SWE as determined from the independent INTAS-SCCONE snow course data over the former Soviet Union. Statistical random error is determined according to (3.3) - (3.9) for different observations and averaged according to (3.10). The systematic error contribution is estimated by (3.2). The observed absolute (residual) error is a sum of these two contributions.

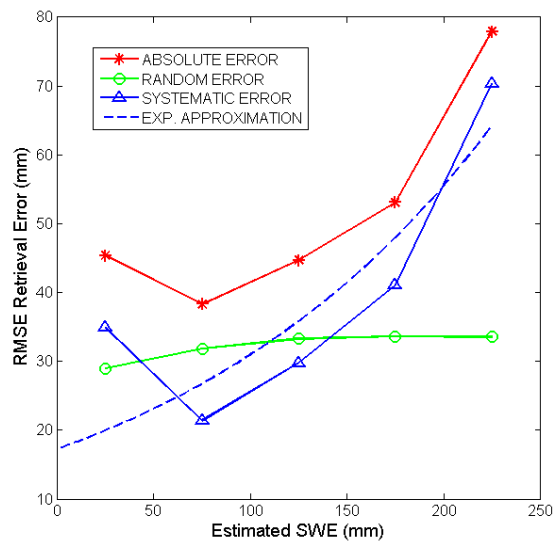


Figure 3.3. Total error of GlobSnow ver.1.3 SWE product as a function of estimated value of SWE (corresponding to Figure 3.2). The depicted curves provide the actual SWE ver.1.3 product accuracy (current product for the SWE retrieval error is the statistical random error depicted by the green line).

3.2.3 Total spatially and temporally varying error of SWE product

Currently, GlobSnow products ver. 1.0, 1.2 and 1.3 only provide the spatially and temporally varying statistical error according to (3.6). As demonstrated by Figure 3.3 for the product version 1.3, this error does not give any realistic figure of the absolute error of the product. However, Figure 3.3 demonstrates that a revised accuracy estimate can be provided in case of product version 1.3 simply by summing the systematic error according to approximation (3.11) with the pixel-wise statistical error using formula (3.3). This product would include the temporal and spatial variability of accuracy, but would on average obey the total error characteristics shown in Figure 3.3.

Further development of SWE product will probably include the separate error characterization for open and forested areas (different accuracy levels for weather station-observed snow depth). If this is carried out, the analysis of Figure 3.3 has to be carried out separately for the two categories.

Future GlobSnow products may also include bias-corrected versions (as the reference data set applied to estimate the retrieval bias is extensive). Figure 3.4 demonstrates the overall behavior of SWE retrieval bias according to (3.4) when the whole INTAS-SCCONE data set is applied to the analysis. Figure 3.4 shows the bias as a function of ground truth reference SWE. Again, the actual product bias has to be presented as a function of estimated SWE. This is shown in Figure 3.5.

In order to obtain bias-corrected SWE estimates the observed bias from Figure 3.5 should be inputted to (3.5) using e.g. an exponential fit function, which is also shown in Figure 3.5. The obtained formula is:

$$BIAS = -22.33 + 37.78 (1 - \exp(-0.0160 SWE)) \quad (3.12)$$

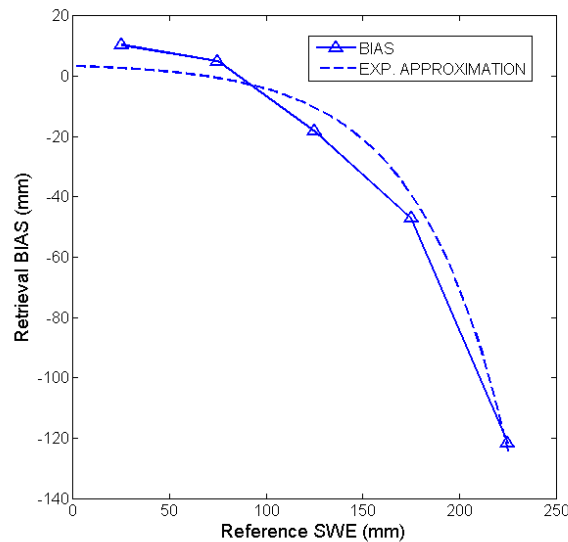


Figure 3.4. GS SWE product ver.1.3 retrieval bias as a function of reference SWE (ground truth).

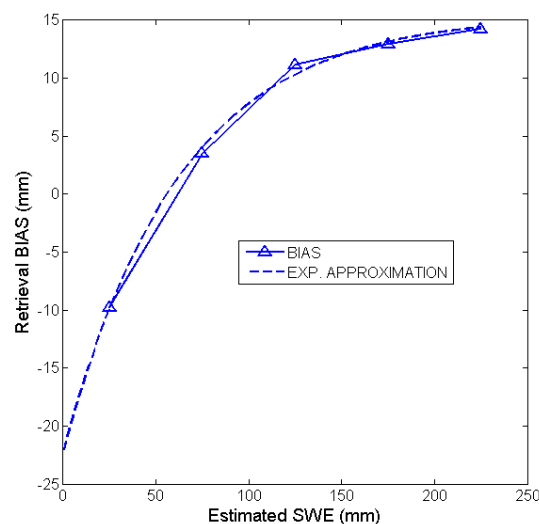


Figure 3.5. GS SWE product ver.1.3 retrieval bias as a function of estimated SWE showing also the exponential fit (3.12) to class-wise averaged data from 147207 reference observations.

The obtained bias, according to Figure 3.5 and the approximation given by (3.12), can be used to provide bias-corrected SWE estimates. Nevertheless, the INTAS-SCCONE SWE data analysis indicates that the influence of bias correction to overall product performance is marginal. This is shown in Figure 3.6. The results also indicate that the bias correction is problematic as it increases SWE estimates that the levels close to 0 mm resulting to a gap in bias-corrected estimates.

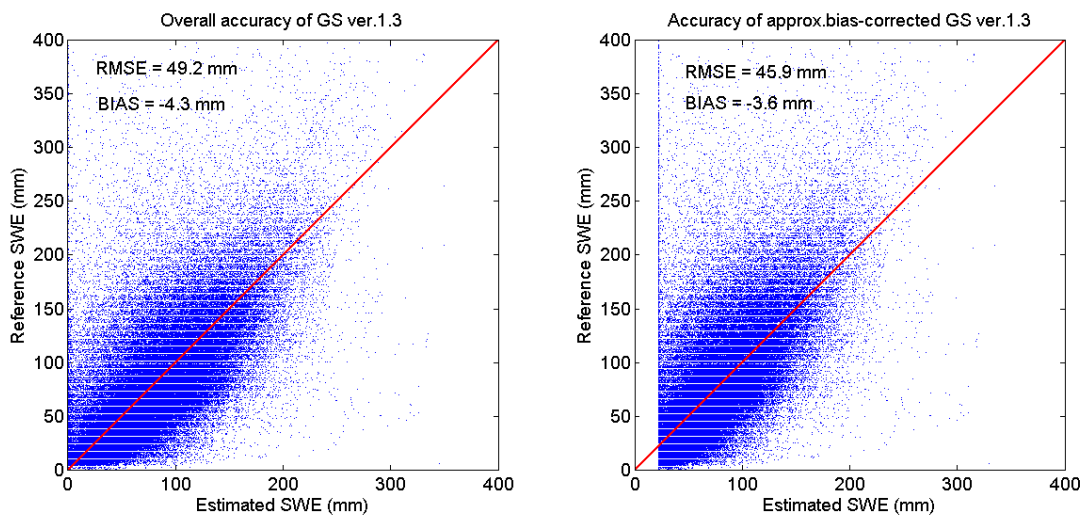


Figure 3.6. Accuracy of the GS SWE-product ver.1.3. Left: Product accuracy through the comparison with independent reference data. Right: Product accuracy is a bias correction according to formula (3.12) is performed. Note that bias correction according to (3.12) increases estimates that show a SWE level of 0 mm with a value of 22.3 mm.

4 CONCLUSIONS

The main modifications to the SWE retrieval algorithm, i.e. changes to the GlobSnow-1 baseline SWE retrieval algorithm v1.3 are summarized in this section.

The new enhancements to the SWE retrieval algorithm are:

- Improved snow emission model (section 2.3.1)
- Variable snow density consideration (section 2.3.2)
- Improved consideration of forests for variable snow density (section 2.3.3)
- Improved uncertainty consideration for SWE (Chapter 3)

The new improvements were implemented to the retrieval algorithm that was used to produce the GlobSnow-2 diagnostic data set (DDS) spanning 2001-2011.

The validation of the new retrieval algorithm (described in this document) is reported in preliminary SWE validation report (GS-2 DEL-8). The initial findings of the validation activities suggest that there may be additional modifications still needed for the SWE retrieval, thus a new version of the ATBD is still possibly foreseen.

5 REFERENCES

Armstrong, R. L., K. W. Knowles, M. J. Brodzik and M. A. Hardman. 1994, updated 2009. DMSP SSM/I Pathfinder daily EASE-Grid brightness temperatures, Jan 1987 – Jul 2008. Boulder, Colorado USA: National Snow and Ice Data Center. Digital media.

Bartalev, S., D. Ershov, A. Isaev, P. Potapov, S. Turubanova, A. Yaroshenko, 2004. Russia's Forests. TerraNorte Information System. RAS Space Research Institute. (<http://terranorte.iki.rssi.ru>).

Brown, R., and P. Mote. 2009. The response of Northern Hemisphere snow cover to a changing climate. *Journal of Climate*. 22: 2124-2145.

Data Announcement 88-MGG-02, Digital relief of the Surface of the Earth. NOAA, National Geophysical Data Center, Boulder, Colorado, 1988. (ETOPO5)

Global Land Cover 2000 database. European Commission, Joint Research Centre, 2003. <http://gem.jrc.ec.europa.eu/products/glc2000/glc2000.php>. (GLC2000)

Hall, D., R. E. J. Kelly, G. A. Riggs, A. T. C. Chang, and J. L. Foster. 2002. Assessment of the relative accuracy of hemispheric-scale snow-cover maps. *Ann. Glaciol.*, vol.34, pp.24–30.

Hallikainen, M., Ulaby, F., and Abdelrazik, M., 1986. Dielectric properties of dry snow in the 3 to 37 GHz range. *IEEE Trans. Antennas Propagat.*, AP-34: 1329-1340.

Hallikainen, M., Ulaby, F., & Deventer, T., 1987. Extinction behavior of dry snow in the 18- to 90-GHz range. *IEEE Transactions on Geoscience and Remote Sensing*, GE-25, 737–745.

Ishimaru, A., 1978. *Wave Propagation and Scattering in Random Media*. New York: Academic, vols. I/II.

Knowles, K., E. Njoku, R. Armstrong, and M.J. Brodzik. 2002. Nimbus-7 SMMR Pathfinder daily EASE-Grid brightness temperatures. Boulder, CO: National Snow and Ice Data Center. Digital media and CD-ROM.

Kontu, A., & Pulliainen, J., 2010. Simulation of spaceborne microwave radiometer measurements of snow cover using in situ data and emission models. *IEEE Transactions on Geoscience and Remote Sensing*, 5, 37–40.

Kruopis, N., Praks, J., Arslan, A., Alasalmi, H., Koskinen, J., & Hallikainen, M., 1999. Passive microwave measurements of snow-covered forests in EMAC'95. *IEEE Transactions on Geoscience and Remote Sensing*, 37, 2699–2705.

Lemmetyinen, J.; Derksen, C.; Pulliainen, J.; Strapp, W.; Toose, P.; Walker, A.; Tauriainen, S.; Pihlflyckt, J.; Karna, J.-P.; Hallikainen, M.T.; , "A Comparison of Airborne Microwave Brightness Temperatures and Snowpack Properties Across the Boreal Forests of Finland and Western Canada," *Geoscience and Remote Sensing, IEEE Transactions on* , vol.47, no.3, pp.965-978, March 2009. doi: 10.1109/TGRS.2008.2006358.

Lemmetyinen, J., Pulliainen, J., Rees, A., Kontu, A., Qiu, Y., and Derksen, C. (2010), Multiple Layer Adaptation of HUT Snow Emission Model: Comparison with Experimental Data. *IEEE Transactions on Geoscience and Remote Sensing*, 48:2781-2794.

Mätzler, C., 1987. Applications of the interaction of microwaves with the natural snow cover. *Remote Sensing Reviews*, 2: 259–387.

Pulliainen, J., J.-P. Kärnä, and M. T. Hallikainen, 1993. Development of geophysical retrieval algorithms for the MIMR. *IEEE Trans. Geosci. Remote Sens.*, 31: 268–277.

Pulliainen, J., J. Grandell, and M. T. Hallikainen., 1999, “HUT Snow Emission Model and its Applicability to Snow Water Equivalent Retrieval”. *IEEE Transactions on Geoscience and Remote Sensing*. 37: 1378-1390.

Pulliainen, J. 2006, “Mapping of snow water equivalent and snow depth in boreal and sub-arctic zones by assimilating space-borne microwave radiometer data and ground-based observations”. *Remote Sensing of Environment*. 101: 257-269.

Salonen, E., S. Karhu, P. Jokela, S. Uppala, S. Sarkkula, and H. Aulamo, 1990. Study of propagation phenomena for low availabilities. Final report under ESTEC Contract 8025/88/NL/PR, Tech. Rep.

Sturm, M., J. Holmgren, and G. Liston. 1995. A seasonal snow cover classification system for local to global applications. *Journal of Climate*. 8: 1261-1283.

Sturm, M., B. Taras, G. Liston, C. Derksen, T. Jonas, and J. Lea. 2010. Estimating snow water equivalent using snow depth data and climate classes. *Journal of Hydrometeorology*. 11: 1380-1394.

Takala, M., Pulliainen, J., Metsämäki, S. and Koskinen, J. 2009 Detection of Snowmelt Using Spaceborne Microwave Radiometer Data in Eurasia From 1979 to 2007. *IEEE Transactions on Geoscience and Remote Sensing*. 47 (9): 2996-3007.

Takala, M., Luojus, K., Pulliainen, J., Derksen, C., Lemmetyinen, J., Kärnä, J.-P., Koskinen, J. and Bojkov, B., 2011, “Estimating northern hemisphere snow water equivalent for climate research through assimilation of space-borne radiometer data and ground-based measurements”, *Remote Sensing of Environment*, 115(12), p. 3517-3529, doi:10.1016/j.rse.2011.08.014.

Tsang L.,J. Pan, D. Liang, Z. Li, D.W.Cline and Y. Tan., 2007. Modeling Active Microwave Remote Sensing of Snow Using Dense Media Radiative Transfer (DMRT) Theory With Multiple-Scattering Effects. *IEEE Transactions on Geoscience and Remote Sensing*, 45(4): 990-1004.

Ulaby F. T., R. K. Moore, and A. K. Fung, 1981. *Microwave Remote Sensing: Active and Passive*. Artech House, Vol. 1.

Weise, T., 1996. Radiometric and structural measurements of snow. Ph.D. dissertation, Inst. Appl. Phys., Univ. of Bern, Switzerland.

Wegmüller, U., & Matzler, C., 1999. Rough bare soil reflectivity model. *IEEE Transactions on Geoscience and Remote Sensing*, 37, 1391–1395.